
Article:
Palma, V., Goodall, R. orcid.org/0000-0003-0720-9694, Thompson, A. et al. (4 more authors) (2021) Ceria-coated replicated aluminium sponges as catalysts for the CO-water gas shift process. International Journal of Hydrogen Energy, 46 (22). pp. 12158-12168. ISSN 0360-3199

https://doi.org/10.1016/j.ijhydene.2020.04.065

Ceria-coated Replicated Aluminium Sponges as Catalysts for the CO-Water Gas Shift Process

Vincenzo Palma[1], Russell Goodall[2], Adam Thompson[3], Concetta Ruocco[1], Simona Renda[1], Richard Leach[3], Marco Martino[1]*

[1]University of Salerno, Department of Industrial Engineering, Via Giovanni Paolo II 132, 84084 Fisciano (SA), Italy

[2]The University of Sheffield, Department of Materials Science & Engineering, Sir Robert Hadfield Building, Portobello St, Sheffield, S1 3JD, UK

[3]Manufacturing Metrology Team, Faculty of Engineering, University of Nottingham, NG8 1BB, UK

mamartino@unisa.it

A study on the use of chemical conversion coating as a preparative technique for foam-based structured catalysts, in the water gas shift reaction, is presented. The results showed a significant correlation between the topological properties of the structure and the preparation technique, highlighting how chemical conversion coating is a suitable technique for highly porous structures. In the first part of the paper, the performance of two structured catalysts obtained by coating commercial aluminium foams, with different porosity, was compared. The activity tests suggested that diffusion phenomena occurred in the case of the uncompressed foams. These results were confirmed by evaluating the performance of a catalyst obtained by coating a compressed 5 PPI pore size commercial aluminium foam, which showed much higher activity, at the same contact time, with respect to the catalyst obtained with the corresponding non-compressed foam. Finally, the performance of a catalyst obtained

by coating an aluminium sponge, synthesized by the replication technique, was compared to that of a catalyst obtained by coating a compressed 40 PPI pore size aluminium foam. The higher activity of the sponge-based catalysts confirmed the dependence of the activity on the topological properties of the structure: X-ray computed tomography images highlighted the narrow distribution of the pore sizes and the presence of “bottleneck type” connections in the sponge structure, which are beneficial for the activity of the catalyst.

Keywords: Water gas shift; Chemical conversion coating; Aluminum foams: Structured catalyst

1. Introduction

Hydrogen is the first and lightest element in the periodic table and, therefore, the most abundant in the universe; its existence, as well as its flammability, have been known since the second half of the eighteenth century. The high abundance of hydrogen, coupled with its high energy density, make it the first candidate to become the energy vector of the next energy transition [1]. Hydrogen can be produced from both fossil and renewable sources [2][3], but the majority is still derived from fossil reserves. The hydrogen first has to be extracted from the fossil source, then it can be used in a fuel cell to generate electrical power [4][5]. Furthermore, problems related to storage [6], transport and security of hydrogen remain partially unresolved. The large-scale centralized production of hydrogen [7], therefore, appears to be difficult, while distributed production is much more attractive [8], as distributed production would considerably limit the problems associated with storage and transport. Unfortunately,

most hydrogen is produced by reforming processes, which, though effective, generate a syngas rich in carbon monoxide; a poison for proton exchange membranes. Therefore, the syngas goes through a series of further transformations, such as two stages of water gas shift [9][10] and one of methanation [11][12], preferential oxidation [13] or a treatment with permselective membranes [14]. The overall process is effective, but inefficient and not suitable for distributed production; where small and smart plants are needed. In recent decades, the attention of many research groups has been focused on the intensification of the CO Water Gas Shift (WGS) process [15] which is clearly, among the process listed above, the most inefficient. The two-stage approach to water gas shift presents several disadvantages: the intermediate cooling phase requires the presence of an auxiliary unit, which adds considerable cost to the process; moreover, the two stages can be considered as two separate processes, further multiplying the costs. In addition, a two-stage process plant is not suitable for the small-scale applications used in distributed hydrogen production. Increasingly sophisticated catalytic formulations [16], proposed in recent years, can be considered competitive alternatives to those actually used in current catalytic systems. In particular, the noble metal-based catalysts supported on reducible oxides, due to the level of catalytic performance, are suitable for the design of single-stage WGS reaction processes [17]. However, these formulations do not solve the underlying problem; that the double-stage process is not efficient. The single-stage process is the only viable way to achieve a robust reduction in costs and plant sizes. A possible solution comes from the use of highly conductive structured carriers, coupled with highly active catalytic formulations [18], i.e. structured catalysts. In the last decades, structured catalysts have been extensively studied, as profitable alternatives to the traditional

powder and pellets catalysts, providing better performance in terms of pressure drops (thus decreasing the energy costs of operation and increasing the lifetime of the catalyst) [19] and heat and mass transfer [20]. In this regard, the development of highly efficient structured catalysts allow processes to be operated in a continuous mode, thus avoiding the barrier towards scaling up [21]. In addition, due to their standard shape and well-defined geometrical and flow properties, foams are highly suitable for easy scale up of the catalytic reactors [22].

One of the main issues related to the use of pellet-shaped catalysts is their inefficient heat conduction, which leads to a disadvantage both in endothermic and exothermic processes: in the first case, temperature gradients along the catalytic bed induce the formation of cold zones that reduce the reaction kinetic; in the latter case, the presence of hot-spots can cause damage to the catalyst and induce its early deactivation. To overcome the limitations of conventional catalysts, higher surface area for the thermal exchange is required, which is normally achieved by using multiple long reactor tubes and/or small diameter, with a negative impact in terms of pressure drops. On the other hand, the route of increasing the diameter of catalyst pellets has a detrimental impact in terms of radial heat transfer, decreased effectiveness factor and more catalyst volume required [23]. Therefore, the high thermal conductivity of the structured carriers plays a key role in the intensification of endothermic and exothermic reaction-based processes, allowing for effective management of the heat of the reaction [24]. In particular, highly conductive carriers may allow the achievement of a pseudo-isothermal profile along the catalytic bed, which is a necessary condition for the realization of a single stage WGS process [25]. Different types of structured carriers have been proposed, such as honeycomb monoliths, open-cell foams and wire meshes.

Among all of the possible geometries, foams appear to be the most promising: comparative studies have shown that open-cell foams provide optimal geometry in many catalytic processes, where tortuosity ensures better axial and radial heat dispersion and mass transfer [26]. In fact, the tortuosity of the structure induces a turbulence in the gas flow which promotes transport phenomena, while other systems such as honeycomb monoliths have ordered channels that split the total flow, thus reaching conditions for laminar flow in each of them. In addition, compared to commercial pelletized catalysts, higher geometrical surface areas are possible, which enhance the activity per unit reactor volume and the external mass transfer rates [27]. Foams can be easily coated with high surface area materials and various well-estabilished technologies are available to do this [28]. Among these, the washcoating technique is the most conventional preparation method; it allows very high active metal loading of the pellets, and thus every pellet catalyst formulation can be replicated with the structured catalyst. In previous studies, the effective thermal conductivity of aluminium foam-based catalysts has been related to the performance, in terms of CO conversion, for the water gas shift reaction [29]. Heat exchange in porous structures is a relatively complex phenomenon, because it takes place in two phases: in the solid network and in the fluid [30]. Many investigations have focused on the correlation between the effective thermal conductivity and the porosity; for high porosity commercial metal foams, it has been suggested that the effective thermal conductivity strongly depends on the cross-sections of the fibre and intersections. However, no systematic dependence has been found on pore density [31]. On the other hand, the effective thermal conductivity of open cell replicated aluminium metal sponges [32], with a porosity (expressed as a fraction of the whole volume) from 0.57 to 0.77 and

pore size between 0.7 mm and 2.4 mm, decreases with increasing porosity, while no pore size influence was found [33]. Another critical issue related to the preparation of structured catalysts is the loading of the active species on the structured carrier. Currently, the most common method to prepare structured catalysts is washcoating: this method consists of loading the carrier with a primer through a colloidal suspension of alumina [34] or silica [35] as a binder. This method involves exploiting the adhesion capacity of these species with the carrier, while the active species can be loaded by mixing with the primer or by subsequent impregnation. This method has been extensively studied over recent decades [36], with the aim of optimizing the procedure. Alternative binders have been proposed, allowing the wide use of structured catalysts, in important industrial processes [37]. Despite its wide use in structured catalysts preparation, washcoating has some disadvantages that affect its use in some cases: it is not suitable for small pore size foams [38] and the resistance to mechanical stresses of the coating depends on the type of binder [39]. Additionally, the primer may not be inert towards the process, and may be detrimental in some cases [40]. Moreover, high specific surface areas can be reached only by loading a large amount of primer and thus, through the formation of too thick a coating. A possible alternative to washcoating is chemical conversion coating, which allows a thin coating of ceria [41], zirconia or titania [42] to be created on aluminium surfaces. This technique has been successfully used in protecting aluminium alloys from corrosion. Moreover it is easy to perform and the resulting coating is highly resistant to mechanical stresses [43] [44]. Conversely, the maximum loading of the protecting species is related to the surface area per unit volume. In previous work, the possibility of using this technique to prepare a ceria-based structured catalyst for the WGS reaction was demonstrated [45].

Ceria is considered an excellent support, thanks to its high oxygen storage capacity [46], in fact it is actively involved in redox behavior and the catalytic activity of the supported catalysts. This leads to improved reaction rates, not only in WGS but also in reforming reactions [47]. It is widely recognized that ceria has the ability to enhance the CO conversion in the WGS reaction because it has a higher redox couple capability than other oxides, due to the high oxygen mobility in the lattice [48]. This mobility, which is related to the oxygen storage capacity, is also responsible for the higher strong metal to support interaction (SMSI) of ceria compared to non-reducible supports [49] [50]. Moreover, CeO_2 has also basic properties, which can inhibit coke formation, resulting in more stable catalysts [51].

Herein, we report a comparative study on some structured catalysts, highlighting the high correlation between the topological properties of the carriers and the activity of the corresponding structured catalysts obtained by chemical conversion coating, with a ceria precursor, followed by impregnation with a platinum precursor, in the CO WGS reaction. Discussion of the activity tests is divided in two parts: in the first part, we discuss the effect of porosity and the relative density of commercial aluminium foams on the activity of the corresponding catalysts in the WGS reaction. In the second part, we compare the activity of a catalyst obtained by coating an opportunely-shaped commercial foam with a catalyst obtained by coating a replicated aluminium sponge.

2. Materials and Methods

2.1 Replicated aluminium sponge preparation

Samples were made by the replication process [52]. Bread flour (Shipton Mill) and NaCl (Fisher Scientific) were blended and mixed with water (in the ratio 70% NaCl, 15% flour and 15% water by mass) to form a dough-like paste. These were then

shaped into spheres of diameter 2.36 mm to 2.80 mm (checked by sieving the spheres to separate those outside this range), and gradually heated up to 973 K in air (held at the maximum temperature for 1 hour) to harden.

The preforms were then placed into a vacuum chamber with a block of 99.85% pure aluminium on top (supplied by William Rowland Ltd, Sheffield, UK). The temperature was raised at 293 K per minute to 1013 K and held at that level for 105 minutes. Argon gas was then let into the chamber up to a pressure of 2.5 bar to cause the aluminium to infiltrate the spaces between the spheres in the preform, and the chamber was cooled under pressure. After solidification, a dissolution treatment in water was used to remove the NaCl, and samples were cut by electro-discharge machining (EDM) into cylinders of length 32 mm, diameter 19 mm and mass 6.9 g.

2.2 Shaping of commercial aluminium foam

The commercial aluminium foam samples studied were prepared by machining from larger blocks of the commercial product (5 PPI, 40 PPI open cell, 10% relative density). The first set of aluminium carriers (designated as Fn, where n = 5, 40 corresponds to the P.P.I. of the foam) was obtained by machining to realize a cylinder with a diameter of 13 mm and a length of 103 mm. Moreover, a 5 PPI foam (size (30×13×103) mm) was compressed and shaped (designated as Fn, where n = 5_C, *n* is the porosity of the parent foam and C identifies that it has been compressed) to make a cylinder with the same size, but with increased relative density. The second set was composed of a replicated aluminium sponge, processed as discussed above, and a foam obtained by compressing and shaping a 40 PPI foam (Fn where n = 40_C) (see Table 1).

Table 1. Textural properties of the structured carriers

Carrier	Length (mm)	Diameter (mm)	Pore size (PPI)	Relative density (%)
F5	103	13	5	10
F40	103	13	40	10
F5_C	103	13	-	29
F40_C	32	19	-	28
R_Sponge	32	19	-	28

2.3 Ceria coating process and catalyst preparation

The aluminium carriers were initially degreased with acetone, then etched with sodium hydroxide solution (1.5 M) for 1 minute and finally treated with nitric acid solution (35 wt%) for 30 s. After each treatment, the carriers were thoroughly washed with distilled water. Immediately after pre-treatment, the carriers were immersed in the bath for coating deposition at a temperature of 323 K for the first set of foams, and at a temperature of 313 K for the latter set. The bath was made by dissolving $CeCl_3 \cdot 7H_2O$ and H_2O_2 35 wt% in distilled water, in a mass ratio 1/3/75, acidified with HCl until a pH of 3 was reached. The chemical treatment was repeated four times for 2 hours; after each treatment the resulting coated carriers were washed with distilled water, the excess of water was removed with compressed air and dried at 393 K for 2 hours. The active metal was then loaded by impregnation of the coated carriers with a solution of tetrammineplatinum (II) nitrate, dried at 393 K for 2 hours and calcined at 723 K for 3 hours.

2.4 Characterization techniques

The coating coverage and active species loading were evaluated by means of energy dispersive X-ray fluorescence (ED-XRF) using an ARL QUANT'X ED-XRF spectrometer (Thermo Scientific). The resistance of the coating to mechanical stress was evaluated using an ultrasound adherence test with an ultrasonic bath CP104 (EIA

S.p.A.). The coated carriers were dipped in ethanol at 298 K and submitted to ultrasound, at 60% of the rated power of the equipment (200 W; 39 kHz), for six cycles of 5 minutes. The XRD diffractograms were obtained with a Brucker D8 Advance, with a Cu Kα radiation source (35 kV; 40 mA) in the 2θ range (20 to 80) °, (Stp = 737; Stp size = 0.0814; t/Stp = 0.5 s). Crystallite dimensions were calculated from the diffractograms by applying the Scherrer equation. The structural changes were evaluated using an inVia Raman microscope (Renishaw), equipped with a 514 nm Ar ion laser operating at 25 mW. Sample morphology was observed by a field emission scanning electron microscope (FE-SEM, mod. LEO 1525, Carl Zeiss SMT AG, Oberkochen, Germany). The H_2-TPR experiments were carried out before the activity tests, with a reducing stream of 500 Ncc/min containing 5 vol% of H_2 in N_2, in the temperature range of 298 K to 723 K, with a heating rate of 10 K/min.

X-ray computed tomography (XCT) measurements were made using a Nikon MCT 225 system with two different scan setups, optimised for each scanned sample. Two samples were obtained by cutting the PtCeR_Sponge and PtCeF40_C exhausted catalysts and these were analyzed by XCT. The scan of the PtCeR_Sponge sample was performed at a geometric magnification of 14×, providing a voxel size of 14.3 μm. The following parameters were used: 3142 X-ray projections formed by averaging two frames per projection, each lasting 2000 ms, a detector gain 24 dB; X-ray tube voltage 115 kV and current 124 μA. The scan of the PtCeF40_C sample was performed at a geometric magnification of 9×, providing a voxel size of 22.2 μm. The following parameters were used: 3142 X-ray projections formed by averaging two frames per projection, each lasting 1425 ms, a detector gain 24 dB; X-ray tube voltage 115 kV and current 191 μA. For both XCT scans, a 0.5 mm copper X-ray pre-filter was used

and a warmup scan of approximately one hour was performed prior to the scan. A detector shading correction was applied by averaging 256 reference frames (128 bright and 128 dark), and flux normalisation was applied during the scan.

XCT data were acquired using Nikon's proprietary acquisition software (X-Inspect) and reconstructed using Nikon's proprietary reconstruction software (CT-Pro). Surface determination was performed on the reconstructed XCT volume in VGStudioMAX 3.2 using the iterative maximum gradient method with the ISO-50 isosurface as a starting point [53], over an initial search distance of 4 voxels. Data were then triangulated and exported from VGStudio using no mesh simplification and imported into MeshLab 2016 for visualisation.

2.5 Catalytic activity tests

The activity tests were performed at atmospheric pressure, in the temperature range of 553 to 673 K, decreasing the temperature in steps, and then by evaluating the products composition when steady state temperature conditions were obtained. The reactor was fed with a reaction mixture of 8 % CO, 30 % H_2O and 62 % N_2, in a stainless steel tubular reactor with an internal diameter of 22 mm and 400 mm length, at a contact time (τ) between 24 ms and 99 ms (GHSV = 36364 - 150000 h^{-1}). The reaction product composition was evaluated, on dry basis, by means of an ABB system equipped with the non-dispersive infrared analyser Uras 14 for CO, CO_2 and CH_4 and a thermal conductivity detector Caldos 17 for H_2.

2.6 Kinetic evaluations

In order to develop a kinetic model able to predict the catalytic behaviour of Al-foams during the WGS reaction, the mass balance equations were written for every component and derived by assuming a steady state and a piston flow of the gas. A

finite increment of 5×10^{-5} g was selected for the catalytic mass in order to ensure that the numerical integration remained stable; the Euler numerical method was used to solve the differential equations and to integrate the system. After the solution of the mass balance, the results of the model were compared with the experimental values, through an objective function which involves the minimization of the differences between the above values through a least-squares method, using the kinetic constants as the variable terms. The model was implemented in the software Microsoft Office Excel 2016.

3. Results and discussion

3.1 Characterization results

The chemical composition of the catalysts was also measured by means of ED-XRF, to evaluate the loading of ceria and platinum (Table 2). The results showed that by increasing the pore density of the foam (5, 40 PPI) an increase of the ceria loading is obtained. This result may be explained by considering that a higher foam surface area per unit volume is available at higher values of PPI (which correspond to smaller pores) [54]. As a consequence of the higher ceria loading, the samples with higher PPI values also showed higher Pt loading. Apart from this effect, the difference in the ceria loading between the compressed and uncompressed F40 foam was attributed to the different coating reaction temperature. The chemical conversion coating is the result of an oxidation reaction between the metallic surface and the salt precursor of the protecting oxide (in our case cerium (III) chloride), so under the same overall reaction conditions, the extent of the coating available for reaction depends on the metallic surface area. The reaction mechanism for the ceria conversion coating provides a series of redox reactions in which the surface aluminium is oxidized in acidic media with the

formation of hydroxyl ions [55]. At the same time, cerium (III) chloride is itself oxidized to give a cerium (IV) hydroxide or peroxide on the aluminium surface and the transformation to cerium (IV) oxide is subsequently obtained by calcining. This technique exploits limited and controlled corrosion to arrive at a material condition which protects against further, unwanted corrosion and, therefore, as the reaction proceeds, the surface is increasingly covered and less and less remaining aluminium can be oxidized. At the same time, the loading is strongly dependent on the reaction temperature, with a higher temperature corresponding to a higher loading. Platinum loading was carried out by impregnation of the coated foams before calcining, in a hot solution of tetramine platinum nitrate. The XRF results showed that the ratio between platinum and ceria was similar for all the catalysts.

Table 2. Catalysts characterization results

Catalyst	Chemical composition (wt%)			Crystallite size (111) (nm)		BET surface area (m^2/g)
	Al	CeO_2	Pt	CeO_2	Pt	
PtCeF5	96.0	3.2	0.4	7.4	35	2.1
PtCeF40	89.0	9.9	1.1	7.8	33	8.1
PtCeF5_C	95.8	3.8	0.4	7.7	32	1.9
PtCeR_Sponge	95.9	3.7	0.4	7.3	22	2.0
PtCeF40_C	90.4	8.7	0.9	7.4	22	7.1

BET surface area measurements showed a progressive increase in the surface area of the structured catalysts with increasing active component loading. From the obtained data, we hypothesized that the surface area of the coating created was about 70 m^2/g. In order to evaluate the resistance of the coating to mechanical stress, the coated carriers were subjected to an ultrasound adherence test, as indicated above. No mass

loss was detected, suggesting the formation of a strongly bonded coating.

XRD diffractograms of the samples showed characteristic peaks for the aluminium carriers (Figure 1), of the cubic ceria fluorite type coated to the aluminium surface. The three peaks at 2θ = 39.9, 46.4 and 67.7 were attributed to platinum. The crystallite size of platinum was also calculated by means of the Scherrer equation (Table 2), highlighting similar sizes for all the catalysts.

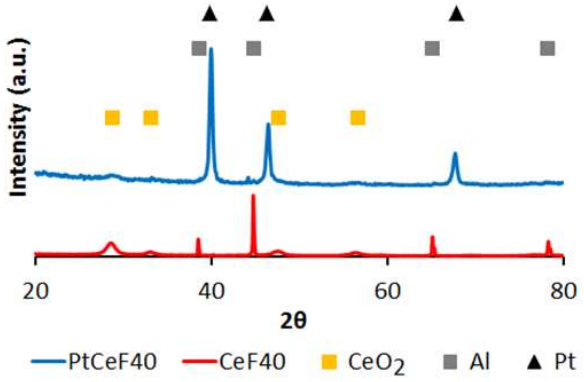

Figure 1. Diffractograms of PtCeF40 and CeF40.

Raman analysis showed that the coated surface of the foams contains a highly defective ceria, while the calcined catalyst clearly shows the formation of the typical cubic fluorite structure (Figure 2). The CeF40 spectrum showed a large peak at about 469 cm^{-1}, which was attributed to the F_{2g} mode typical of a fluorite-type cubic structure. This peak corresponds to the symmetrical stretching of oxygen around Ce^{4+}. The two bands at approximately 270 cm^{-1} and 600 cm^{-1} were attributed respectively to the second-order transverse acoustic mode (2TA) and the defect induced mode (D) of ceria. It has been observed that these defects promote the catalytic activity of ceria, as they regulate the oxygen storage capacity of the support, through the redox cycles between the species Ce^{4+} and Ce^{3+} [56][57]. The peak at 842 cm^{-1} has been attributed to the stretching of the O-O bonds of the peroxide species [58]. This identification supports the reaction mechanism previously proposed, according to which ceria is

formed in the presence of H_2O_2 and there is subsequent decomposition of $Ce(O_2)(OH)_2$ at high temperature. The PtCeF40 spectrum showed two peaks at 461 cm^{-1} and 516 cm^{-1}. The 461 cm^{-1} peak was ascribed once again to F_{2g} mode, while the peak at 516 cm^{-1} was attributed to the interaction with platinum [59].

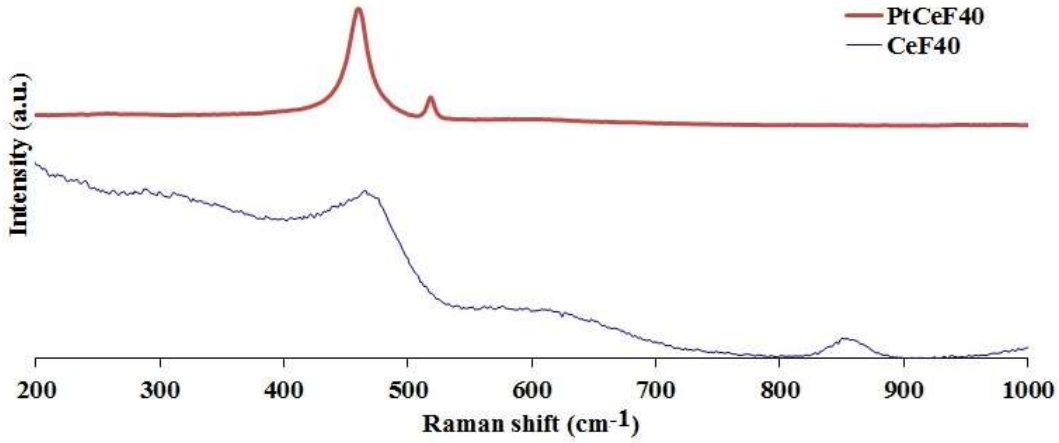

Figure 2. Raman spectra of PtCeF40 and CeF40

The SEM image of the coated foams highlighted the nanometric morphology of the coating. Moreover, canal-like or fracture-like cavities are present, which could be beneficial structures to increase the catalytic activity (Figure 3).

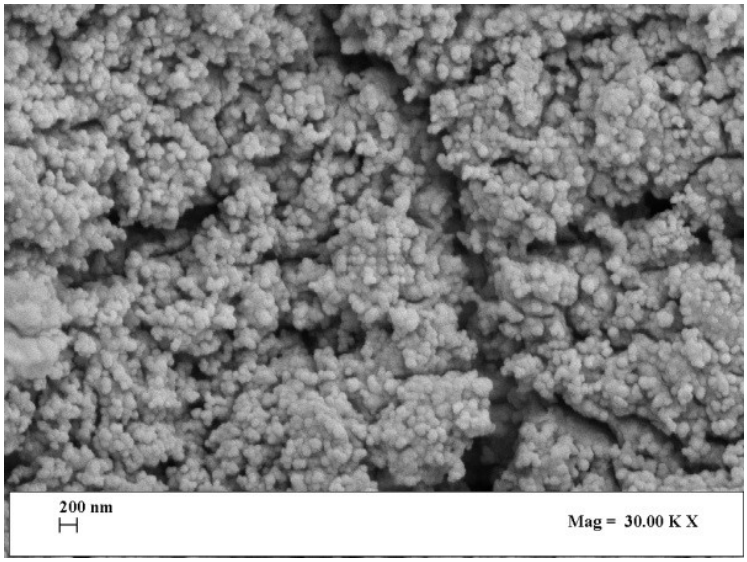

Figure 3. SEM image of CeF40

Good coverage of the surface with ceria and the good dispersion of metallic platinum were indicated by the EDS imaging. The distribution of aluminium on the surface shows that the majority of the surface is covered by ceria and that there are no cerium-free islands.

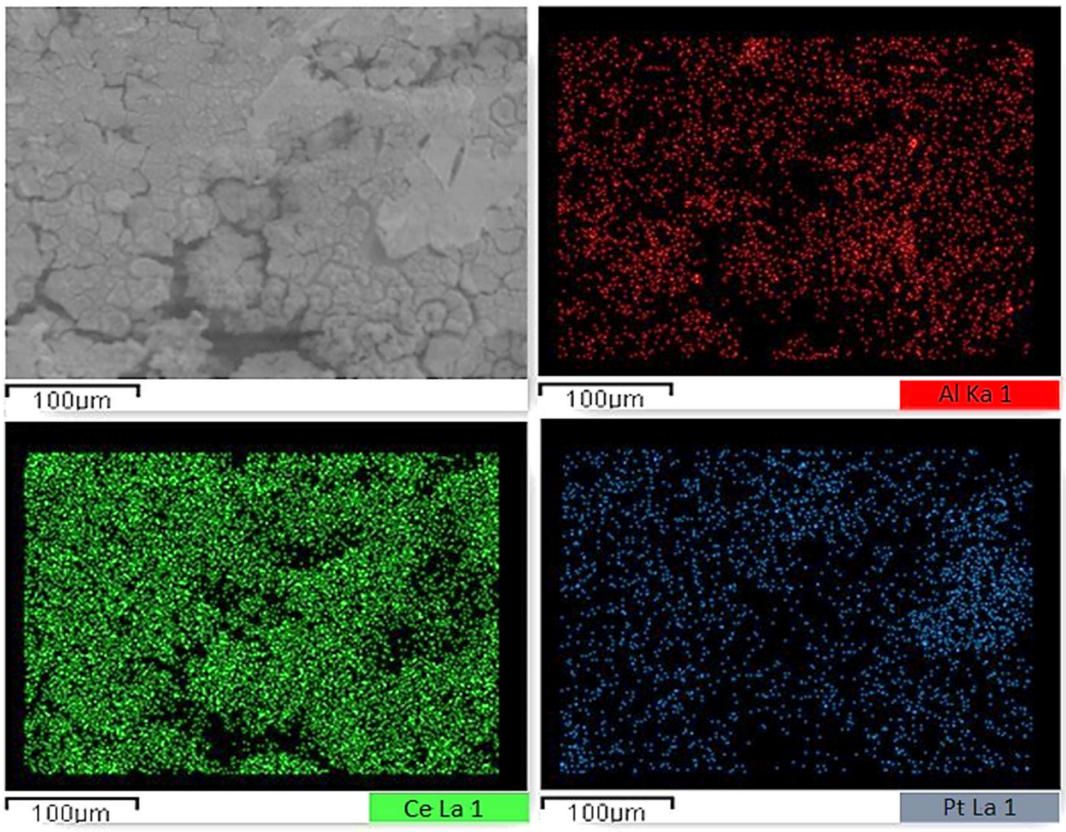

Figure 4. EDS of PtCeF40

While the platinum distribution is satisfactory, the ratio between platinum and cerium is not constant throughout the image. This factor implies an imperfect dispersion, attributed to the method used in the platinum impregnation (see Figure 4).

3.2 Activity tests results

In a preliminary comparison, the activity of the two structured catalysts PtCeFn with n = 5, 40 was evaluated by performing the tests at the same contact time (τ = 30 ms).

For all the catalysts, the results showed a progressive reduction of the CO conversion with increasing temperature (see Figure 5 A).

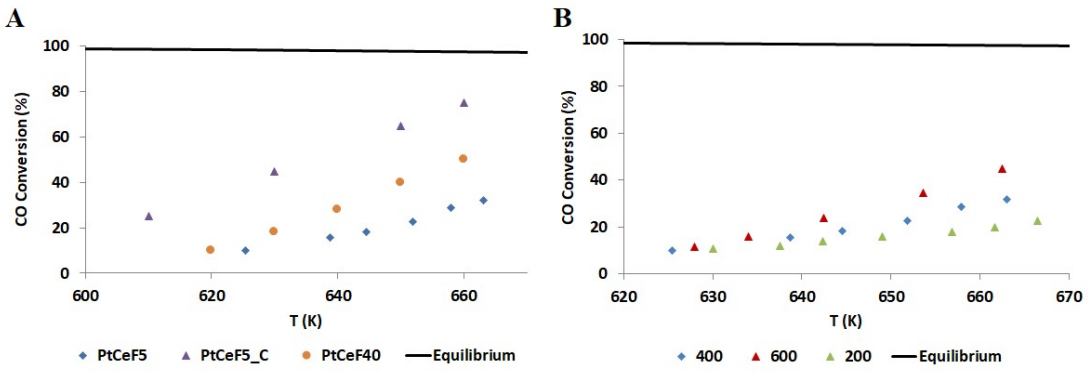

Figure 5. CO conversion as function of temperature at τ= 30 ms, feeding conditions: 8%CO, 30% H_2O, 62% N_2, P=1 atm. Comparison among the PtCeFn catalysts with n=5, 40, 5_C (A) and PtCeF5 catalyst at three different flow rate: 200, 400 and 600 Ncc/min (B).

By comparing the performances of the two uncompressed catalysts, the foam having a smaller pore diameter (PtCeF40) displayed slightly increased CO conversion. These results suggest a correlation between the porosity of the foam and the catalytic activity. In fact, two main phenomena were relevant; the reaction and the mass transport within the foam. The latter phenomenon was dominant in the case of the PtCeF5, whose lower CO conversion showed that the chemical reaction is not controlling the process in this case. This problem may be due instead to an insufficient diffusion of the reactant within the catalytic bed. This hypothesis is suggested by the fact that, in the case of PtCeF40, an enhanced CO conversion was obtained by increasing the temperature; this foam, in fact, has a smaller pore dimension, which forces the gas distribution into the structure and increases the local gas velocity. As such, a higher turbulence in the flow (and, therefore, better diffusion) is achieved. To experimentally verify the eventual external diffusion limitation, the PtCeF5 sample was prepared at three

different catalytic masses and tested under three flow-rates: 200, 400 and 600 Ncc/min, by maintaining the same hourly gas space velocity, as well as contact time. The results, shown in Figure 5 (B), demonstrate that, at temperatures lower than 640 K, when the gas velocity though the catalytic bed is changed, the CO conversion remains the same. On the other hand, at higher temperatures, the contribution of diffusion is more pronounced compared to that of the chemical reaction. These results also explain the similar trend of the curves for PtCeF5 and PtCeF40 observed below 640 K in Figure 5 (A). To better explore this phenomenon, as mentioned above, an aluminium foam of size (30 × 13 × 103) mm and porosity 5 PPI, was compressed with a bench vice in the radial direction, to obtain a cylindrical structure with 13 mm diameter and 103 mm length. The pressed structure was coated, and the performance of the resulting catalyst compared to the corresponding PtCeFn catalyst (Figure 5 (A)). The CO conversion exceeded 75% at 673 K and reached 25% at 610 K. The compression of the carrier increased the relative density of the foam, deforming the pores and generating something similar to a dense wire mesh. Thus, a great increase of the tortuosity was achieved and the huge turbulence created in the reduced size pores gave a boost to the reaction.

In the second part of this work, the activity of a catalyst obtained by coating a compressed 40 PPI aluminium foam (PtCeF40_C) was compared with a catalyst obtained by coating a replicated aluminium sponge (PtCeR_Sponge), with the same relative density, as described in section 2.1; the activity test results were compared in terms of the reaction rate. For both the catalysts investigated in this work, the kinetic constant k of the WGS reaction was calculated on the base of the Arrehnius equation by optimizing the pre-exponential factor and the activation energy values following

the rate expression used in previous work [21], under the hypothesis of first-order dependency on the CO and H_2O reactants. (Eq.1, where K_{eq} is the equilibrium constant calculated through the GasEQ tools and P_i refers to the partial pressure of the various components). This assumption, which is coherent with the experimental data, was also used by other authors for CeO_2-based catalysts [60].

$$r = k\left(P_{CO}P_{H2O} - \frac{1}{K_{eq}}P_{CO2}P_{H2}\right). \quad \text{Eq. 1}$$

From the slope and the intercept of the fitting line, it was possible to evaluate the kinetic expression (activation energy and pre-exponential value, respectively) and the values found for the two samples are shown in Table 3.

Table 3. Kinetic parameters

Sample	Activation Energy ($kJ \cdot mol^{-1}$)	Pre-exponential factor ($kmol \cdot s^{-1} \cdot atm^{-2}$)
PtCeR_Sponge	100	1758
PtCeF40_C	104	1195

Very close activation energies were calculated for the two catalysts, implying that the difference is coherent with the experimental error. Moreover, the activation energy found for the Pt-based catalyst of the present report is coherent with the values reported for similar catalytic systems in the recent literature [61]. The CO reaction rate (rCO, $mol_{CO} \cdot g_{cat}^{-1} \cdot s^{-1}$) was calculated according to previously reported expressions [62]. A comparison between the two catalysts at different contact times was undertaken, and in

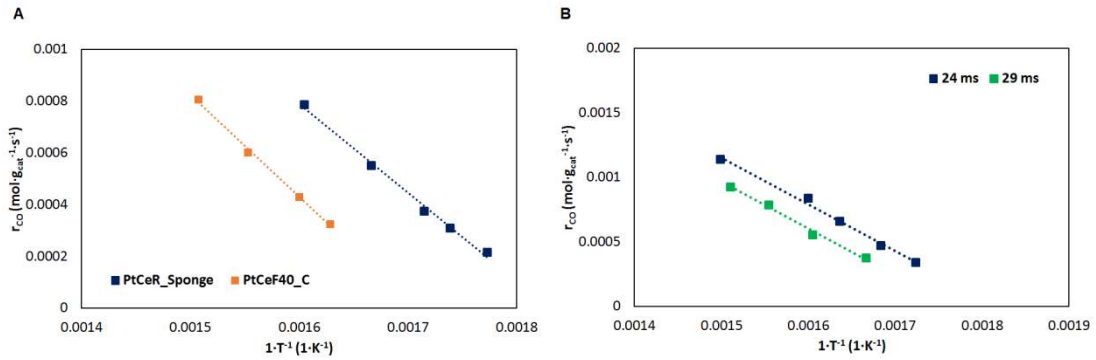

Figure 6, the result at 29 ms is reported. From the obtained data, it is clear that the prediction of the first-order expression is in agreement with the experimental values; moreover, for all the investigated contact times, the CO reaction rate measured for the PtCeR_Sponge was higher than that observed over the PtCeF40_C catalyst. The time on stream experiment carried out on the PtCeR_Sponge catalyst (see Figure 7), showed a high stability of this catalyst: less than 10% of CO conversion was lost during the first 8 hours of reaction, while in the following hours the conversion remained stable.

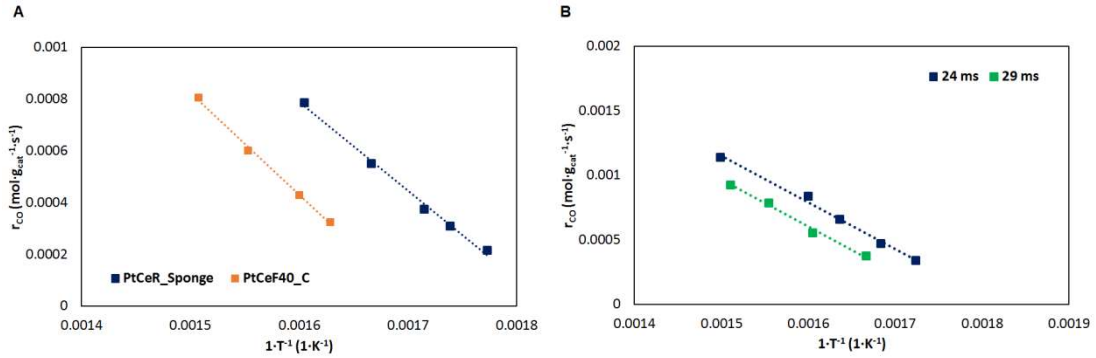

Figure 6. Arrhenius plots of kinetic reaction rates; feeding conditions: 8%CO, 30% H_2O, 62% N_2, P=1 atm. (A) Comparison between PtCeR_Sponge and PtCeF40_C at a contact time of 29 ms. (B) Comparison between two contact times (24 ms and 29 ms) for PtCeR_Sponge.

After 35 hours, a cycle of oxidation (TPO) and reduction (H_2-TPR) was performed without affecting the CO conversion in the following experiment.

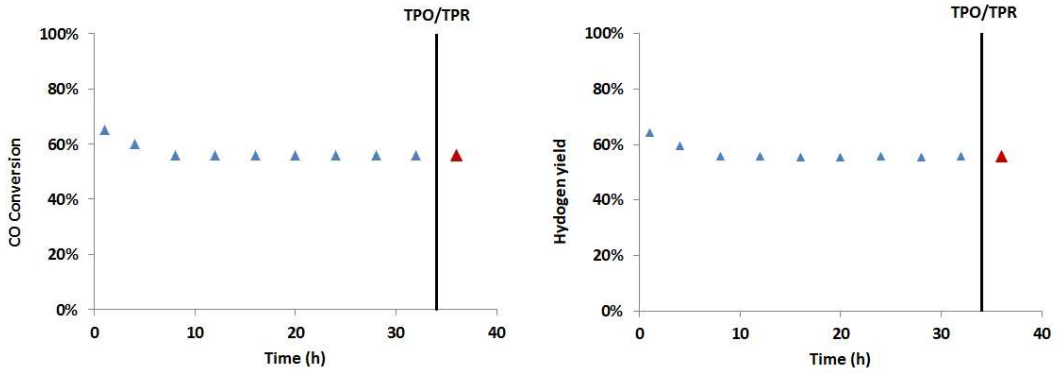

Figure 7. Time on stream on PtCeR_Sponge catalyst. Feeding conditions: 8%CO, 30% H2O, 62% N2, P=1 atm, T= 593 K, τ= 38 ms

In all tests, no methanation occurred, such that high selectivity to hydrogen was achieved. The activity tests results confirmed that the textural characteristics of the structure can affect the performance of the catalysts. In Figure 8, images of the XCT data of the two catalysts are reported. These images highlight the physical differences between the two structures: the pores of the sponge had a spherical form, and small openings between the pores, while in the compressed foam it was impossible to define the individual pores.

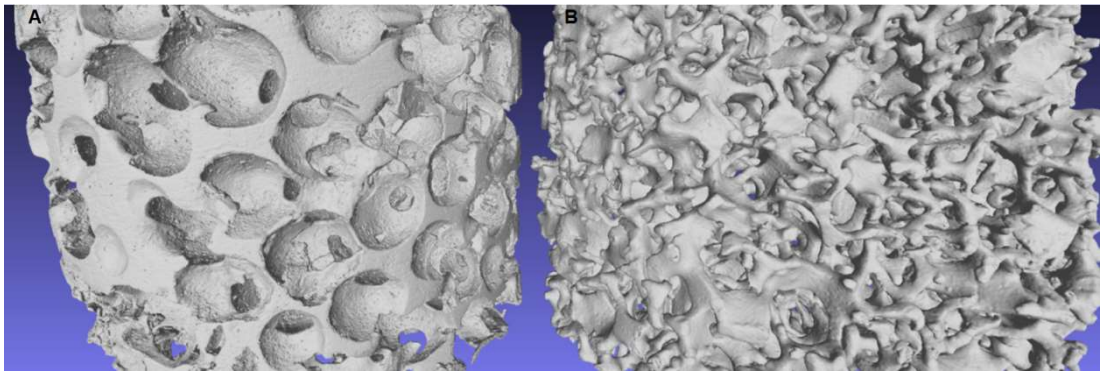

Figure 8. 3D XCT images of PtCeR_Sponge (A) and PtCeF40_C (B). Lateral view.

However, pseudo-elliptical cavities can be identified in the compressed foam structures, formed from the initial porous structure as the result of the compression. Moreover, the compression process seems to have distorted the structure in an uneven manner. Nevertheless, as can be seen in the XCT data, the pores of the sponge are

interconnected with smaller channels through which the gas is forced to flow. The top view of a segment of the two structures highlights the difference between the void distribution in the two cases (Figure 9).

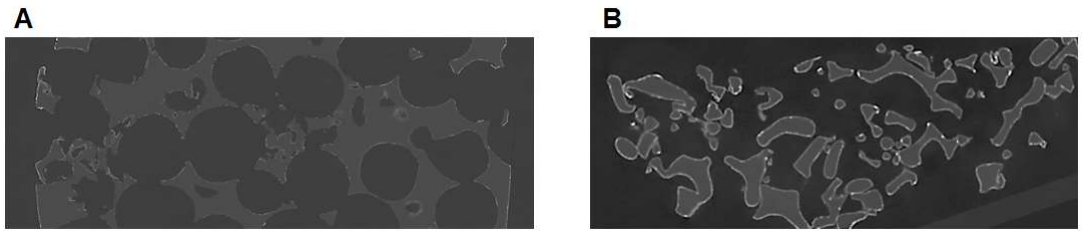

Figure 9. "D XCT slice data of PtCeR_Sponge (A) and PtCeF40_C (B). View from the top.

The pores in the sponge have a limited number of small connections with the adjacent pores, giving rise to "bottleneck"-type structures (see Figure 9A) [63], which could be beneficial in catalytic systems. By contrast, the structure of the compressed foam is more open and the distribution of the void spaces through the entire volume is disordered, generating preferential directions for flow (Figure 9B), that are detrimental for catalysis applications.

Conclusions

In the first part of this paper, we compared the activity of structured catalysts prepared by chemical conversion coating of commercial open cell aluminium foams with different porosities in the WGS reaction. The activity tests showed that diffusion phenomena occurred in the case of the uncompressed foams. In the second part of this work, we compared the activity of two structured catalysts obtained by coating two different structures. In one case, the structure was obtained by compressing a commercial open cell aluminium foam; in the other case the structure was obtained by producing a different open cell foam through a replication process. The results showed better performance for the catalysts obtained using the replicated sponge. XCT

analysis highlighted a different distribution of the pores in the structures: the sponge was characterized by a regular distribution of spheroidal pores with limited interconnection, while the compressed foam was characterized by an irregular structure in which the compression was not able to completely eliminate the preferential directions. On the basis of these results, we can conclude that:

1. The chemical conversion coating is not an alternative technique to washcoating; rather, it is a technique that can be used in highly porous systems, where washcoating would not be feasible. On the other hand, the choice of the coating technique is intimately related to the textural characteristics of the structure.
2. The replication process can be considered to be a highly suitable technique for sponge preparation as it allows design and creation of porous structures under controlled conditions. The narrow distribution of porosities and "bottleneck"-type connections can prevent the formation of preferential directions, obtaining benefits in the field of catalysis. Conversely, the simple compression of commercial structure does not guarantee the elimination of bypass phenomena.

Acknowledgments

The authors wish to acknowledge Mariarosa Scognamiglio (Department of Industrial Engineering, University of Salerno) for SEM-EDS analysis, Ing. Angela Russo and Ing. Chiara Esposito for their valuable contribution, and Dr Faye Senior, Dept. Materials Science & Engineering, University of Sheffield, for assistance with the production of the metallic foam samples. RG would like to acknowledge a Fellowship supported by the RAEng/Leverhulme Trust Senior Research Felloships Scheme. AT and RKL would like to thank EPSRC (Grant EP/M008983/1) for funding this work.

References

[1] Acar C, Bicer Y, Demir ME, Dincer I. Transition to a new era with light-based hydrogen production for a carbon-free society: An overview. Int J Hydrogen Energy 2019;44:25347-25364. https://doi.org/10.1016/j.ijhydene.2019.08.010.

[2] Jokar SM, Rahimpour MR, Shariati A, Iulianelli A, Bagnato G, Vita A, Dalena F, Basile A. Pure Hydrogen Production in Membrane Reactor with Mixed Reforming Reaction by Utilizing Waste Gas: A Case Study. Processes 2016;4(3):33. https://doi.org/10.3390/pr4030033.

[3] Iulianelli A, Palma V, Bagnato G, Ruocco C, Huang Y, Veziroğlu NT, Basile A. From bioethanol exploitation to high grade hydrogen generation: Steam reforming promoted by a Co-Pt catalyst in a Pd-based membrane reactor. Renew Energy 2018;119:834-843. https://doi.org/10.1016/j.renene.2017.10.050.

[4] Liu X, Reddi K, Elgowainy A, Lohse-Busch H, Wang M, Rustagi N. Comparison of well-to-wheels energy use and emissions of a hydrogen fuel cell electric vehicle relative to a conventional gasoline-powered internal combustion engine vehicle. Int J Hydrogen Energy 2020;45:972-983. https://doi.org/10.1016/j.ijhydene.2019.10.192.

[5] Evrin RA, Dincer I. Thermodynamic analysis and assessment of an integrated hydrogen fuel cell system for ships. Int J Hydrogen Energy 2019;44:6919-6928. https://doi.org/10.1016/j.ijhydene.2019.01.097.

[6] Tavhare P, Kalamse V, Krishna R, Titus E, Chaudhari A. Hydrogen adsorption on Ce-ethylene complex using quantum chemical methods. Int J Hydrogen Energy 2016;41(27):11730-11735. https://doi.org/10.1016/j.ijhydene.2015.11.172.

[7] Mosca L, Medrano Jimenez JA, Assefa Wassie S, Gallucci F, Palo E, Colozzi M, Taraschi S, Galdieri G. Process design for green hydrogen production, International Journal of Hydrogen Energy. In press, https://doi.org/10.1016/j.ijhydene.2019.08.206.

[8] Stefan Czernik, Richard French, Distributed production of hydrogen by auto-thermal reforming of fast pyrolysis bio-oil, Int J Hydrogen Energy 2014;39:744-750. https://doi.org/10.1016/j.ijhydene.2013.10.134.

[9] Bosch C, Wild W. 1914, CA153379 (A).

[10] Dienes EK. 1967, US3303001 A.

[11] Zyryanova MM, Snytnikov PV, Amosov YI, Ven'yaminov SA, Golosman EZ, Sobyanin VA. Selective methanation of CO in the presence of CO_2 in hydrogen-containing mixtures on nickel catalysts. Kinet Catal 2010;51:907–913. https://doi.org/10.1134/S0023158410060170.

[12] Zhang M, Yu F, Li J, Chen K, Yao Y, Li P, Zhu M, Shi Y, Wang Q, Guo X. High CO Methanation Performance of Two-Dimensional Ni/MgAl Layered Double Oxide with Enhanced Oxygen Vacancies via Flash Nanoprecipitation. Catalysts 2018;8(9):363. https://doi.org/10.3390/catal8090363.

[13] Wootsch A, Descorme C, Duprez D. Preferential oxidation of carbon monoxide in the presence of hydrogen (PROX) over ceria–zirconia and alumina-supported Pt catalysts. J Catal 2004;225:259–266. https://doi.org/10.1016/j.jcat.2004.04.017.

[14] Fernandez E, Helmi A, Coenen K, Melendez J, Viviente JL, Pacheco Tanaka DA, Van Sint Annaland M, Gallucci F. Development of thin Pd–Ag supported

membranes for fluidized bed membrane reactors including WGS related gases. Int J Hydrogen Energy 2015;40:3506–3519. https://doi.org/10.1016/j.ijhydene.2014.08.074.
[15] García-Moncada N, González-Castaño M, Ivanova S, Centeno MA, Romero-Sarria F, Odriozola JA. New concept for old reaction: Novel WGS catalyst design, Appl Cat B-Environ 2018;238:1-5. https://doi.org/10.1016/j.apcatb.2018.06.068.
[16] Carta D, Montini T, Casula MF, Monai M, Bullita S, Fornasiero P, Corrias A. The water gas shift reaction over Pt–CeO_2 nanoparticles confined within mesoporous SBA-16. J Mater Chem A 2017;5:20024-20034. https://doi.org/10.1039/C7TA03640J.
[17] Hwang K-R, Park J-S, Ihm S-K. Si-modified Pt/CeO_2 catalyst for a single-stage water-gas shift reaction. Int J Hydrogen Energy 2011;36(16):9685-9693. https://doi.org/10.1016/j.ijhydene.2011.05.065.
[18] Palma V, Pisano D, Martino M. Structured noble metal-based catalysts for the WGS process intensification. Int J Hydrogen Energy 2018;43:11745-11754. https://doi.org/10.1016/j.ijhydene.2018.01.085.
[19] Kolaczkowski ST, Awdry S, Smith T, Thomas D, Torkuhl L, Kolvenbach R. Catal Today 2016;273:221-233. https://doi.org/10.1016/j.cattod.2016.03.047.
[20] Tronconi E, Groppi G, Visconti CG. Structured catalysts for non-adiabatic applications. Curr Opin Chem Eng 2014;5:55–67. https://doi.org/10.1016/j.coche.2014.04.003.
[21] Ou X, Pilitsis F, Xu N, Taylor SFR, Warren J, Garforth A, Zhang J, Hardacre C, Jiao Y, Fan X. On developing ferrisilicate catalysts supported on silicon carbide (SiC) foam catalysts for continuous catalytic wet peroxide oxidation (CWPO) reactions. Catal Today 2018;in press. https://doi.org/10.1016/j.cattod.2018.06.033.
[22] Duprez D, Cavani F. Handbook of Advanced Methods and Processes in Oxidation Catalysis. London: Imperial College Press: 2014. https://doi.org/10.1142/p791.
[23] Twigg MV, Richardson JT. Fundamentals and Applications of Structured Ceramic Foam Catalysts. Ind Eng Chem Res 2007;46(12): 4166-4177. https://doi.org/10.1021/ie061122o.
[24] Palma V, Pisano D, Martino M. CFD modeling of the influence of carrier thermal conductivity for structured catalysts in the WGS reaction. Chem Eng Sci 2018;178:1–11. https://doi.org/10.1016/j.ces.2017.12.035.
[25] van Dijk HAJ, Boon J, Nyqvist RN, van den Brink R.W. Development of a single stage heat integrated water–gas shift reactor for fuel processing. Chem Eng J 2010;159:182–189. https://doi.org/10.1016/j.cej.2010.02.046.
[26] Palma V, Pisano D, Martino M. Comparative Study Between Aluminum Monolith and Foam as Carriers for The Intensification of The CO Water Gas Shift Process. Catalysts 2018;8:489. http://dx.doi.org/10.3390/catal8110489.
[27] Palma V, Ruocco C, Ricca A. Ceramic foams coated with PtNi/CeO_2ZrO_2 for bioethanol steam reforming. Int J hydrogen Energy 2016;41(27):11526-11536. https://doi.org/10.1016/j.ijhydene.2016.04.028.
[28] Twigg MV, Richardson JT. Theory and Applications of Ceramic Foam Catalysts. Chem Eng Res Des 2002;80(2):183-189. https://doi.org/10.1205/026387602753501906.

[29] Palma V, Pisano D, Martino M. The influence of the textural properties of aluminum foams as catalyst carriers for water gas shift process. Int J Hydrogen Energy 2017;42(37):23517-23525. http://dx.doi.org/10.1016/j.ijhydene.2017.04.003.
[30] Calmidi VV, Mahajan RL. The effective thermal conductivity of high porosity fibrous metal foams. J Heat Transfer 1999;121(2):466–471. http://dx.doi.org/10.1115/1.2826001.
[31] Bhattacharya A, Calmidi VV, Mahajan RL. Thermophysical properties of high porosity metal foams. Int J Heat Mass Transfer 2002;45:1017-1031. https://doi.org/10.1016/S0017-9310(01)00220-4.
[32] Elizondo Luna EM, Barari F, Woolley R, Goodall R. Casting protocols for the production of open cell aluminum foams by the replication technique and the effect on porosity. J Vis Exp 2014;94:article number e52268. https://doi.org/10.3791/52268.
[33] Abuserwal AF, Elizondo Luna EM, Goodall R, Woolley R. The effective thermal conductivity of open cell replicated aluminium metal sponges. Int J Heat Mass Transfer 2017;108:1439–1448. http://dx.doi.org/10.1016/j.ijheatmasstransfer.2017.01.023.
[34] Cristiani C, Finocchio E, Latorrata S, Visconti CG, Bianchi E, Tronconi E, Groppi G, Pollesel P. Activation of metallic open-cell foams via washcoat deposition of Ni/$MgAl_2O_4$ catalysts for steam reforming reaction. Catal Today 2012;197(1):256-264. https://doi.org/10.1016/j.cattod.2012.09.003.
[35] Mitra B, Kunzru D. Washcoating of Different Zeolites on Cordierite Monoliths. J Am Chem Soc 2008;91(1):64-70. https://doi.org/10.1111/j.1551-2916.2007.02032.x.
[36] Cristiani C, Visconti CG, Finocchio E, Gallo Stampino P, Forzatti P. Towards the rationalization of the washcoating process conditions Catal Today 2009;147:s24-S29. https://doi.org/10.1016/j.cattod.2009.07.031.
[37] Balzarotti R, Cristiani C, Francis LF. Combined dip-coating/spin-coating depositions on ceramic honeycomb monoliths for structured catalysts preparation. Catal Today 2019; 334:90-95. https://doi.org/10.1016/j.cattod.2019.01.037.
[38] Ho PH, Ambrosetti M, Groppi G, Tronconi E, Jaroszewicz J, Ospitali F, Rodríguez-Castellón E, Fornasari G, Vaccari A, Benito P. One-step electrodeposition of Pd–CeO_2 on high pore density foams for environmental catalytic processes. Catal Sci Technol 2018;8:4678-4689. http://dx.doi.org/10.1039/C8CY01388H.
[39] Rao N, Anamika P, Deepak Kunzru M. Washcoating of γ-alumina on stainless steel microchannels, Catal Today 2009;147:S17-S23. https://doi.org/10.1016/j.cattod.2009.07.026.
[40] Palma V, Pisano D, Martino M. Structured noble metal-based catalysts for the WGS process intensification. Int J Hydrogen Energy 2018;43:11745-11754. https://doi.org/10.1016/j.ijhydene.2018.01.085.
[41] Hughes AE, Taylor RJ, Hinton BRW, Wilson L. XPS and SEM Characterization of Hydrated Cerium Oxide Conversion Coatings. Surf Interface Anal 1995;23:540 – 550. https://doi.org/10.1002/sia.740230714.

[42] Milosev I, Frankel GS. Review—Conversion Coatings Based on Zirconium and/or Titanium. J Electrochem Soc 2018;165(3):C127-C144. https://doi.org/10.1149/2.0371803jes.
[43] Dabalà M, Armelao L, Buchberger A, Calliari I. Cerium-based conversion layers on aluminum alloys. Appl Surf Sci 2001;172:312-322. https://doi.org/10.1016/S0169-4332(00)00873-4.
[44] Bethencourt M, Botana FJ, Cano MJ, Marcos M. Advanced generation of green conversion coatings for aluminium alloys. Appl Surf Sci 2004;238:278–281. https://doi.org/10.1016/j.apsusc.2004.05.268.
[45] Palma V, Martino M, Truda L. Nano-CeO_2 Coating on Aluminum Foam Carriers for Structured Catalysts Preparation. Chemical Engineering Transactions 2019;73:127-132. https://doi.org/10.3303/CET1973022.
[46] Jurković DL, Pohar A, Dasireddy VDBC, Likozar B. Effect of Copper-based Catalyst Support on Reverse Water-Gas Shift Reaction (RWGS) Activity for CO_2 Reduction. Chem Eng Technol 2017;40(5):973-980. https://doi.org/10.1002/ceat.201600594.
[47] Pohar A, Hočevar S, Likozar B, Levec J. Synthesis and characterization of gallium-promoted copper–ceria catalyst and its application for methanol steam reforming in a packed bed reactor. Catal Today 2015;256:358-364. https://doi.org/10.1016/j.cattod.2015.01.043.
[48] Jeong D-W, Jang W-J, Shim J-O, Han W-B, Roh H-S, Jung UH, Yoon WL. Low-temperature water–gas shift reaction over supported Cu catalysts. Renewable Energy 2014;65:102-107. https://doi.org/10.1016/j.renene.2013.07.035.
[49] Koo KY, Roh H, Jung UH, Wang LY. CeO_2 Promoted Ni/Al_2O_3 Catalyst in Combined Steam and Carbon Dioxide Reforming of Methane for Gas to Liquid (GTL) Process. Catal Lett 2009;130:217. https://doi.org/10.1007/s10562-009-9867-4.
[50] Huang T, Lin H, Yu T. A Comparison of Oxygen-vacancy Effect on Activity Behaviors of Carbon Dioxide and Steam Reforming of Methane over Supported Nickel Catalysts. Catal Lett 2005;105:239–247. https://doi.org/10.1007/s10562-005-8697-2.
[51] Fonseca Lucrédio A, Jerkiewickz G, Moreira Assaf E. Nickel catalysts promoted with cerium and lanthanum to reduce carbon formation in partial oxidation of methane reactions. Appl Cat A-Gen 2007;333(1):90-95. https://doi.org/10.1016/j.apcata.2007.09.009.
[52] Goodall R, Mortensen A, "Microcellular Aluminium? - Child's Play!", Adv Eng Mater 2007;9(11):951-954. https://doi.org/10.1002/adem.200700190.
[53] Kiekens K, Welkenhuyzen F, Tan Y, Bleys P, Voet A, Kruth J-P, Dewulf W. A test object with parallel grooves for calibration and accuracy assessment of industrial computed tomography (CT) metrology. Meas Sci Technol 2011;22:115502. https://doi.org/10.1088/0957-0233/22/11/115502.
[54] http://ergaerospace.com/technical-data/surface-area-of-duocel-foam/
[55] Decroly A, Petitjean J-P. Study of the deposition of cerium oxide by conversion on to aluminum alloys, Surf Coat Technol 2005;194:1-9. https://doi.org/10.1016/j.surfcoat.2004.05.012.

[56] Daniel M, Loridant S. Probing reoxidation sites by in situ Raman spectroscopy: differences between reduced CeO_2 and Pt/CeO_2. J Raman Spectrosc 2012;43:1312. http://dx.doi.org/10.1002/jrs.4030.
[57] Palma V, Ruocco C, Meloni E, Gallucci F, Ricca A. Enhancing $Pt\text{-}Ni/CeO_2$ performances for ethanol reforming by catalyst supporting on high surface silica, Catal Today 2018;307:175-188. https://doi.org/10.1016/j.cattod.2017.05.034
[58] Christoph T. Nottbohm, Christian Hess, Investigation of ceria by combined Raman, UV–vis and X-ray photoelectron spectroscopy, Catalysis Communications, 22, 2012, 39-42.
[59] Liu H-H, Wang Y, Jia A-P, Wang S-Y, Luo M-F, Lu J-Q. Oxygen vacancy promoted CO oxidation over Pt/CeO_2 catalysts: a reaction at $Pt\text{-}CeO_2$ interface. Appl Surf Sci 2014;314:725. http://dx.doi.org/10.1016/j.apsusc.2014.06.196.
[60] Bobrova L, Andreev D, Ivanov E, Mezentseva N, Simonov M, Makarshin L, Gribovskii A, Sadykov V. Water–Gas Shift Reaction over Ni/CeO_2 Catalysts. Catalysts 2017;7(10):310. https://doi.org/10.3390/catal7100310.
[61] del Villar V, Barrio L, Arash H, Van Sint Annaland M, Gallucci F, Fierro JLG, Navarro RMN. Effect of Re addition on the WGS activity and stability of $Pt/CeO_2–TiO_2$ catalyst for membrane reactor applications. Catal Today 2016;268:95-102. https://doi.org/10.1016/j.cattod.2015.11.013.
[62] Han, Y.; Xue-Tao, Q.; Yue, Y.; Yun-Fei, T.; Zhao, J.; Chun-Jiang, J. Promoted Cu Fe_3O_4 catalysts for low-temperature water gas shift reaction: Optimization of Cu content. Appl Cat B-Environmental 2017;211:137-147. https://doi.org/10.1016/j.apcatb.2017.12.050.
[63] Otaru AJ, Morvan HP, Kennedy AR. Measurement and simulation of pressure drop across replicated porous aluminium in the Darcy-Forchheimer regime. Acta Materialia 2018;149:265-273. https://doi.org/10.1016/j.actamat.2018.02.051.